Supporting Information

Improving the Hole Mobility of Conjugated Semiconducting Polymer Film by Fast Backbone Aggregation during Film Formation Process

Tianya Jin[1,2], Jichen Li[1], Hongxiang Li[3]*, Xinyu Liu[1,2], Junhang Li[1,2], Qiang Zhang[1], Xinhong Yu[1], Xiaozheng Duan[1]*, and Yanchun Han[1,2]*

[1]State Key Laboratory of Polymer Physics and Chemistry, Changchun Institute of Applied Chemistry, Chinese Academy of Sciences, 5625 Renmin Street, Changchun 130022, P. R. China

[2]School of Applied Chemistry and Engineering, University of Science and Technology of China, Hefei 230026, P. R. China

[3]College of Polymer Science and Engineering State Key Laboratory of Polymer Materials Engineering, Sichuan University, Chengdu 610065, P. R. China

* To whom correspondence should be addressed

Tel: 86-431-85262175. Fax: 86-431-85262126

Email: lihongxiang@scu.edu.cn (Hongxiang Li); xzduan@ciac.ac.cn (Xiaozheng Duan); ychan@ciac.ac.cn (Yanchun Han)

Supporting Information contents

1. The calculation method and detailed data of GIWAXS

2. GISAXS Model Fitting

3. The Hansen solubility parameter of IDTBT and solvents

4. The detailed data of in-suit UV-vis absorption

5. The Molecular Dynamics Simulation of IDTBT solution and film

6. The charge mobility of IDTBT

1. The calculation method and detailed data of GIWAXS

GIWAXS is a common and effective technique in the field of conjugated polymer films. By analyzing the 2D patterns, we can extract much information about molecular packings, such as the molecular packing distance, coherence length, and relative degree of crystallinity (rDoC). When an incident X-ray plane wave passes through the film, part of it is diffracted by the periodic plane of an atom or molecule. A spot of high intensity is provided by the constructive interference of reflections of order packing structure. The Angle at which diffraction occurs is related to the distance between the planes, and the direction of the diffracted beam is related to the direction of the planes. The magnitude of the scattering vector is:

$$q = \left(\frac{4\pi}{\lambda}\right)\sin\theta \tag{1}$$

During the testing process, the wavelength λ of the X-ray is given by the synchrotron radiation facility, and the scattering angle 2θ is set according to the experimental requirements. Bragg condition is:

$$q = \frac{2\pi}{d_{hkl}} \tag{2}$$

where d_{hkl} is the packing distance, and q is the peak position. The shape of the diffraction peak is closely related to the size of the molecular packing. The full width at half maximum (FWHM) reflects the size of the molecules packing. The coherence length can be extracted to evaluate the grain size by the Scherrer equation,

$$L_c = \frac{2\pi \mathrm{K}}{FWHM} \tag{3}$$

where K factor about the shape of diffraction. rDoC is a convenient parameter to use to qualitatively compare the degree of molecular packing. To measure rDoC, the peaks need to be integrated completely from out-of-plane to in-plane direction to get the pole figure, as shown in Figure S1. The degree of crystallinity (DoC) is proportional to the integrated intensity of the pole figure, so the rDoC is the ratio of the integrated intensity to the maximum of the strength integral. The integrated intensity is:

$$\frac{\Delta\beta\Delta\theta}{2\pi}[I_{peak} - I_{baseline}] + \int_0^{\pi/2} \sin(\chi) I(\chi) d\chi \tag{4}$$

where Δβ is the horizontal (out of the scattering plane) acceptance angle, Δθ is the vertical (in the scattering plane) resolution, I_{peak} is the maximum intensity of the resolution limited peak, $I_{baseline}$ is the baseline intensity of the resolution limited peak, χ is the polar angle, sin(χ) term is used to explain for the decrement of intensity with increasing χ resulting from the GIXD geometry.[1]

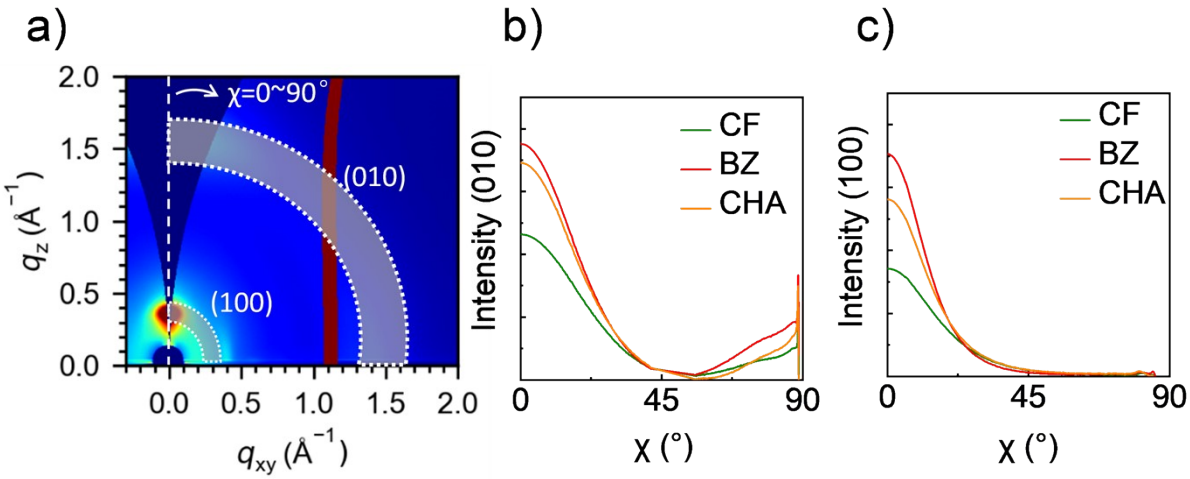

Figure S1. The calculation method of rDoC. a) The schematic of integrating the diffraction peak completely. The pole figure of b) (100) peak and c) (010) peak.

Table S1. The peak position (q), packing distance (d-spacing), FWHM, and coherence length of out-of-plane (100) and (010) peaks and in-plane (001) and (010) peaks.

	Out-of-plane (100)			
	q (Å^{-1})	d-spacing (Å)	FWHM (Å^{-1})	Coherence length (Å)
chloroform	0.37	16.97	0.1570	35.60
benzene	0.35	17.94	0.1290	43.33
cyclohexane	0.35	17.94	0.1460	38.28

	Out-of-plane (010)			
	q (Å^{-1})	d-spacing (Å)	FWHM (Å^{-1})	Coherence length (Å)
chloroform	1.50	4.19	0.3940	14.19
benzene	1.52	4.13	0.3438	16.26
cyclohexane	1.51	4.16	0.3677	15.20

	In-plane (001)			
	q	d-spacing	FWHM	Coherence length

	(Å^{-1})	(Å)	(Å^{-1})	(Å)
chloroform	0.40	15.70	0.0769	72.68
benzene	0.40	15.70	0.0664	84.17
cyclohexane	0.40	15.70	0.0692	80.77

	In-plane (010)			
	q (Å^{-1})	d-spacing (Å)	FWHM (Å^{-1})	Coherence length (Å)
chloroform	1.38	4.55	0.4141	13.50
benzene	1.41	4.45	0.4084	13.69
cyclohexane	1.40	4.49	0.4115	13.58

2. GISAXS Model Fitting

To analyze the aggregation size of IDTBT films prepared by chloroform, benzene, and cyclohexane solutions, the universal model was used to fit the GISAXS 1D profiles that describe the scattering contribution of the aggregation domain (as seen in **Equation 5**). The data was fitted by the software SasView (Version 5.04).

$$I(q) = \frac{A_1}{\left[1 + (q\xi)^2\right]^2} + A_2\langle P(q,R)\rangle S(q,R,\eta,D) + B \#(5)$$

$$S(q) = 1 + \frac{\sin\left[(D-1)tan^{-1}(q\eta)\right] b + \sqrt{b^2 - 4ac}}{(qR)^D} \quad \frac{D\Gamma(D-1)}{\left[1 + \frac{1}{(q\eta)^2}\right]^{(D-1)/2}} \#(6)$$

where q represents the scattering wave vector, A_1, A_2, and B are independent fitting parameters. Debye-Andersone-Brumberger (DAB) is the first term, and the average correlation length of the unaggregated domain is represented by ξ. The contribution from fractal-like aggregations of aggregated domain is the second term. P (q, R) is the form factor of aggregated domain, and S (q, R, η, D) means the fractal structure factor. In this fractal-like aggregation system, the interchain between primary particles is described by the S (q, R, η, D), where R is the mean spherical radius of primary aggregated domain particles, η is the correlation length of the fractal-like structure, and D is the fractal dimension of the aggregation. The **Equation 7** is used to obtain the Guinier radius of the fractal-like aggregation R_g that estimates the average domain size.

$$R_g = \eta\sqrt{\frac{D(D+1)}{2}} \#(7)$$

3. The Hansen solubility parameter of IDTBT and solvents

Donor-acceptor (D-A) conjugated polymers have similar structures. The backbones are composed of fused rings and the side chains are composed of large and branched alkyl chains. Because there are obvious distinctions of structures between backbone and side chains, some solvents exhibit mutual solution for both the backbone and the side chain and some solvents exhibit selective solubility to one of them. To quantify the interaction between the backbone and side chain of the polymer and the solvent, Hansen solubility parameter distance (R_a) was usually used, as shown in **Equation 8**.

$$R_a^2 = 4(\delta_{d1} - \delta_{d2})^2 + (\delta_{p1} - \delta_{p2})^2 + (\delta_{h1} - \delta_{h2})^2 \quad (8)$$

In the equation, dispersion force (δ_d), dipolar chain force (δ_p), and hydrogen bonding (δ_h) of polymer and solvents are necessary. The solubility parameter of solvents can be easily obtained by looking up the Hansen Solubility Parameters Handbook.[2] The solubility parameters of the backbone and side chain of IDTBT were calculated by the HSPiP software (Figure S1). The solubility parameter and the R_a values of solvents to the backbone and side chain of IDTBT are shown in Table S2.

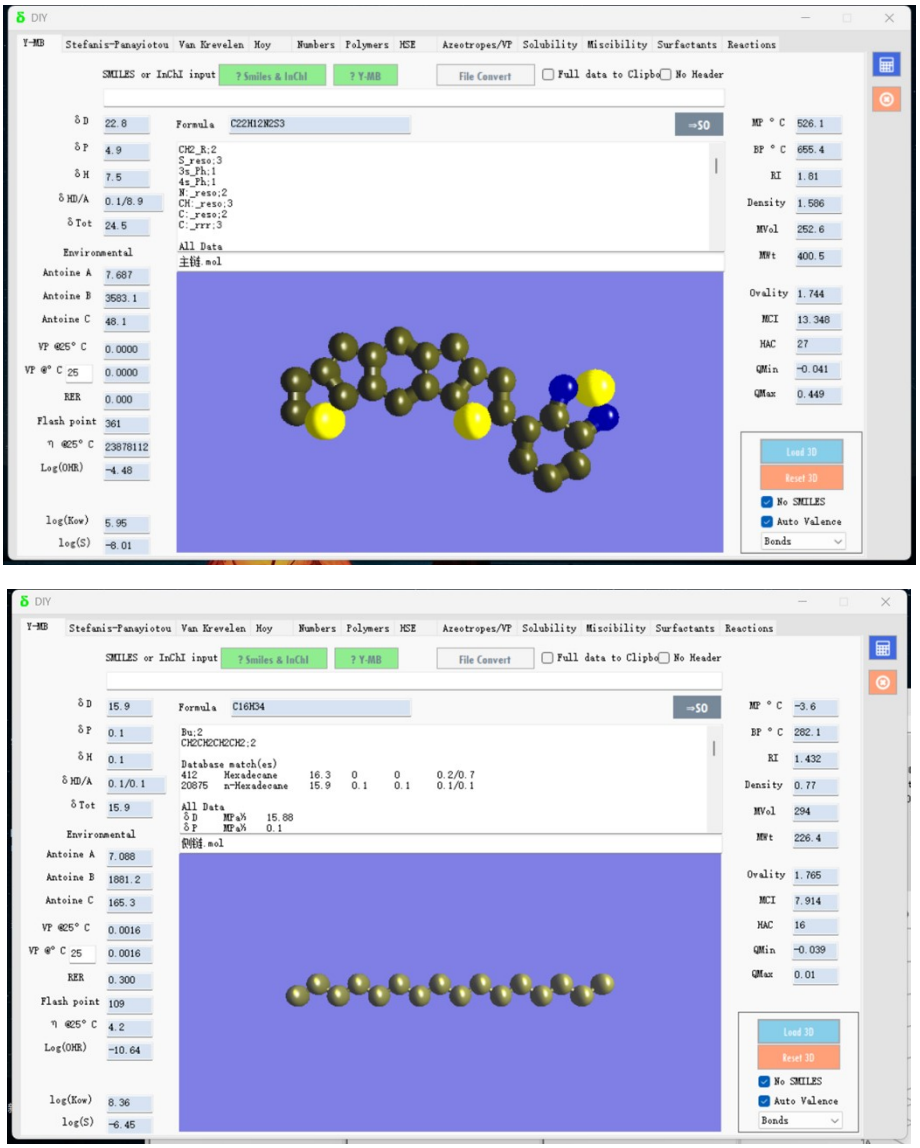

Figure S1. The parameter coordinates of IDTBT backbone and side chain that calculated by HSPiP software.

Table S2. The solubility parameters (δ_d, δ_p, and δ_h) of IDTBT backbone, side chain, and solvents. R_a between solvents and IDTBT backbone and side chain.

	Solvents	δ_d $(J/cm^3)^{1/2}$	δ_p $(J/cm^3)^{1/2}$	δ_h $(J/cm^3)^{1/2}$	$R_{a(b)}$[a] $(MPa^{1/2})$	$R_{a(s)}$[b] $(MPa^{1/2})$
Polar solvent	chloroform	17.8	3.10	5.70	10.32	7.40
Nonpolar solvent	benzene	18.40	0	2.00	11.48	5.35
	cyclohexane	16.80	0	0.20	14.88	1.81
IDTBT	backbone	22.80	4.90	7.50	-	-
	side chain	15.90	0.10	0.10	-	-

a) The Hansen solubility parameter distance between solvent and backbone; b) The Hansen solubility parameter distance between solvent and side chain.

4. The detailed data of in-suit UV-vis absorption

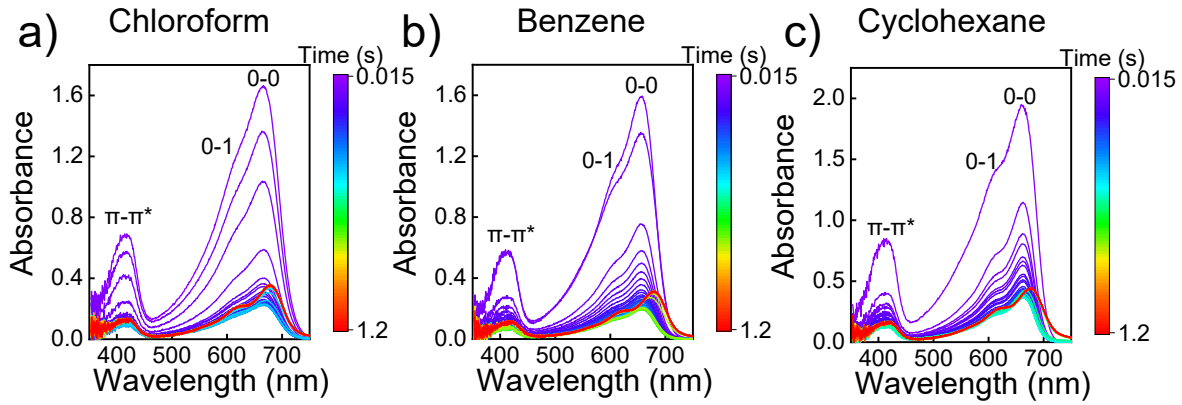

Figure S2. The original data of in situ UV-vis absorption. UV-vis absorption spectra of IDTBT from solution to film that dissolved by a) chloroform, b) benzene, and c) cyclohexane.

5. The Molecular Dynamics Simulation of IDTBT solution and film

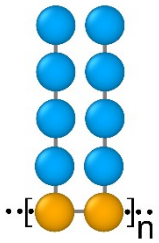

Figure S3. Schematic illustration of a coarse-grained IDTBT molecule, with the backbone in orange and the grafted sidechains in blue.

Molecular Dynamics Simulation

We use Molecular Dynamics (MD) simulation to study the structural properties of the IDTBT polymers under different solvent conditions. The model used here is developed based on our previous simulation studies and other references[3-14]. In the simulation, each IDTBT polymer is coarse-grained as a grafted chain consisting of a sequence of conjunctive spherical beads. As illustrated in Figure S1, the orange beads indicate the IDTBT backbones and the blue ones represent the grafted sidechains, respectively. In this work, we set the polymerization degree of each polymer as n = 60, which is comparable with the IDTBT polymer used in our experimental studies. For computational simplicity, we fix the diameters of all beads to be σ = 1.0, which corresponds to 4 Å. In our simulation, the implicit model is employed to reflect the effects of the solvents. The van der Waals between beads is modeled through the Lennard-Jones (LJ) potential,

$$U_{LJ}(r) = \begin{cases} 4\varepsilon\left[\left(\frac{\sigma}{r}\right)^{12} - \left(\frac{\sigma}{r}\right)^{6} + S\right], r \le r_c \\ 0, r > r_c \end{cases} \quad (10)$$

where ε indicates the energetic parameter and σ represents the size parameters, respectively. In this model, the increase in ε can reflect the stronger attractions between backbone or sidechains caused by the deteriorated solubility of the solvents. In the case of IDTBT solutions, the energetic parameters between polymer components are adjusted from 1.0 ~ 1.5 (which corresponds to 1.0 ~ 1.5 $k_B T$ at room temperature T = 298 K). In the case of IDTBT films, the energetic parameters between polymer components are adjusted from 1.0 ~ 2.0

(which corresponds to 1.0 ~ 2.0 k_BT). We change the cutoff from $r_c = 1.0\sigma$ to $r_c = 2.0\sigma$ and shift the LJ potential to 0 at r_c by *S*. In the simulations, $\epsilon = 1.0$ (which corresponds *to* k_BT at room temperature) and $\sigma = 1.0$ (which corresponds to 4 Å) are used as the energy length and units, respectively. Further, we use the finitely extensible nonlinear elastic (FENE) potential to model the bonded interactions between the conjunctive beads using,

$$U_{FENE}(r_b) = -\frac{1}{2}kR_0^2 \ln\left[1 - \left(\frac{r_b}{R_0}\right)^2\right] \quad (11)$$

where $k = 30\ \epsilon_0/\sigma^2$ indicates the spring constant and $R_0 = 1.5\ \sigma$ represents the maximum bond extension. In addition, we employ the harmonic angle potential to model the intrinsic chain rigidity of the IDTBT backbones,

$$U_{Angle}(\theta) = \kappa_a(\theta - \theta_0)^2 \quad (12)$$

in which θ is the angle of connected beads (i-1, i and i +1), θ_0 is set as 180° and $\kappa_a = 10$.

We perform all simulations in a canonical (NVT) ensemble with the 3D periodic boundary conditions using the Large-scale Atomic/Molecular Massively Parallel Simulator (LAMMPS) package[15]. For the case of IDTBT solutions, we put 40 IDTBT polymers in a cubic simulation box with the size of $L = 50\ \sigma$, so that the monomer concentration of IDTBT polymers is comparable to our experiments. For the case of IDTBT film, we put 20 IDTBT polymers in a cubic simulation box with the size of $L = 24\ \sigma$, so that the number density of the monomers is controlled as 0.85. For all the simulations, we set the integration MD time step as $t = 0.005$ (which corresponds to 10 fs in the real units) and control the temperature at $T =$ 298K using the Langevin thermostat. We first perform the simulations for 10^6 MD steps for the system equilibration, after which we further perform the simulation for another 10^6 MD steps for ensemble analysis. For each system, we perform 20 parallel simulations with different initial configurations and collect the final results from the order of 10^3 to 10^4 statistically independent samples.

6. The charge mobility of IDTBT films

Table S3. The charge mobility summary of IDTBT films cast from different solvents in literature

Solvents	M_n (kDa)	M_w (kDa)	PDI	Mobility ($cm^2\ V^{-1}\ s^{-1}$)	Reference
chlorobenzene	38	108	2.84	1.0±0.25	*J. AM. CHEM. SOC.* **2010**, *132*, 11437–11439
chlorobenzene	38	108	2.84	1.2 (μ_{max})	*Macromolecules* **2011**, *44*, 6649–6652
chlorobenzene	80	160	2.00	2.0±0.20	*Nat. Commun.* **2013**, *4*, 2238
	58.3	95.3	1.63	1.5	*J. Am. Chem. Soc.* **2019**, *141*, 18806−18813
chlorobenzene	108.6	295.4	2.72	1.8	*Adv. Funct. Mater.* **2019**, *29*, 1905340
chloroform	112	340	3.00	1.95±0.22	*J.Mater.Chem.C* **2020**, *8*, 15646
chloroform	9	14.4	1.6	2.96×10^{-2}	*Macromolecules* **2020**, *53*, 7511−7518
75% O-dichlorobenzene + 25% chloroform	69	116	1.68	1	*Adv. Electron. Mater.* **2021**, 2101019
chloroform	112	340	3.04	0.75	*Macromolecules* **2022**, *55*, 297−308
toluene				1.11	
chlorobenzene				1.15	
chlorobenzene	338.4	1049	3.10	2.25	*Macromolecules* **2021**, *54*, 9896−9905
O-dichlorobenzene				1	*Nat. Commun.* **2022**, *13*, 3076

REFERENCES

1. J. Rivnay, S. C. B. Mannsfeld, C. E. Miller, A. Salleo and M. F. Toney, *Chem. Rev.*, 2012, **112**, 5488-5519.
2. C. M. Hansen, *Hansen solubility parameters: a user's handbook.*, CRC press:, 2007.
3. T. Li, C. Liang, K. Yu, J. Li, C. Lin, H. Li, Y. Xu, S. Cai, Q. Zhu, Q. Huang, W. Xing and X. Duan, *Phys. Chem. Chem. Phys.*, 2023, **25**, 28272-28281.
4. J. Liang, H. Wei, K. Yu, C. Lin, H. Li, M. Ding and X. Duan, *Soft Matter*, 2021, **17**, 6305-6314.
5. S. J. Marrink, H. Jelger Risselada, Serge Yefimov, D. P. Tieleman and A. H. d. Vries, *J. Phys. Chem. B*, 2007, **111**, 7812-7824.
6. C. Lin, H. Wei, H. Li and X. Duan, *Soft Matter*, 2022, **18**, 1603-1616.
7. H. Huo, W. Zhao, X. Duan and Z.-Y. Sun, *Macromolecules*, 2023, **56**, 1065-1076.
8. X. Duan, A.-C. Shi and L. An, *Macromolecules*, 2021, **54**, 9053-9062.
9. B. Liu, B. Hu, J. Du, D. Cheng, H.-Y. Zang, X. Ge, H. Tan, Y. Wang, X. Duan, Z. Jin, W. Zhang, Y. Li and Z. Su, *Angew. Chem.*, 2021, **133**, 6141-6150.
10. Z. Zhu, X. Duan, Q. Li, R. Wu, Y. Wang and B. li, *J. Am. Chem. Soc.*, 2020, **142**, 4481-4492.
11. B. Li, X. Duan, D. Cheng, X. Chen, Z. Gao, W. Ren, K.-Z. Shao and H.-Y. Zang, *J. Am. Chem. Soc.*, 2022, **145**, 2243-2251.
12. Z.-D. Wang, S. Liang, Y. Yang, Z.-N. Liu, X.-Z. Duan, X. Li, T. Liu and H.-Y. Zang, *Nat. Commun.*, 2023, **14**, 1-7.
13. L. Yao, C. Lin, X. Duan, X. Ming, Z. Chen, H. Zhu, S. Zhu and Q. Zhang, *Nat. Commun.*, 2023, **14**, 1-10.
14. R. Chen, T. Jin, Y. Liu, T. Zhang, X. Liu, L. Zhang, Y. Chen, H. Li, X. Duan and Y. Han, *Macromolecules*, 2023, **56**, 5356-5368.
15. S. Plimpton, *J. Comput. Phys.*, 1995, **117**, 1-19.